Chinese Physics Letters **41**, 084205 (2024) **Express Letter**

Turbulent Image Restoration in Atmosphere with Cyclopean Processing via Binocular Fusion

Han Yao(姚涵)[1], Jin-Yan Lin(林锦演)[1], Li-Bang Chen(陈立邦)[2], Yi-Kun Liu(刘忆琨)[2], and Jian-Ying Zhou(周建英)[1*]

[1]*State Key Laboratory of Optoelectronic Materials and Technologies, School of Physics, Sun Yat-Sen University, Guangzhou 510275, China*
[2]*Guangdong Provincial Key Laboratory of Quantum Metrology and Sensing, School of Physics and Astronomy, Sun Yat-Sen University (Zhuhai Campus), Zhuhai 519082, China*

(Received 3 June 2024; accepted manuscript online 30 July 2024)

The outstanding issue to overcoming atmospheric turbulence on distant imaging is a fundamental interest and technological challenge. We propose a novel scenario and technique to restore the optical image in turbulent environmental by referring to Cyclopean image with binocular vision. With human visual intelligence, image distortion resulting from the turbulence is shown to be substantially suppressed. Numerical simulation results taking into account of the atmospheric turbulence, optical image system, image sensors, display and binocular vision perception are presented to demonstrate the robustness of the image restoration, which is compared with a single channel planar optical imaging and sensing. Experiment involving binocular telescope, image recording and the stereo-image display is conducted and good agreement is obtained between the simulation with perceptive experience. A natural extension of the scenario is to enhance the capability of anti-vibration or anti-shaking for general optical imaging with Cyclopean image.

DOI: 10.1088/0256-307X/41/8/084205

The impact of atmospheric turbulence on long-distance optical imaging is an important research topic as its application is widespread in various fields. Atmospheric turbulence causes random fluctuations in air density hence the refractive index. This variability in the refractive index alters the path of light traveling through the atmosphere, giving rise to the uncontrolled bending of the light rays.[1] As a result, the turbulence leads to image blurring and distortion, significantly degrading the quality of the imaging.[2,3] There has been a great deal of effort to overcome the turbulence effect, among which adaptive optics is most effective for mitigating the turbulence. The adaptive technology utilizes a series of optical components to correct distortions in the wavefront of light entering the optical system.[4,5] However, the adaptive equipment is rather complex and needs to have very fast response time to compensate the time-varying distortion. Image post-processing is an alternative technology for dealing with the effects of atmospheric turbulence, including image fusion,[6] lucky imaging,[7] point spread function (PSF) correction,[8,9] and deep learning.[10,11] However, image post-processing presents limited capability apart from the required substantial computational resources and processing time depending on the complexity and validity of the technique.

We show in this work that the turbulence effect can be effectively suppressed with binocular fusion via Cyclopean image, or Allelotropia.[12] Cyclopean image is a single mental image of a scene created by the brain through the process of combining two images received from both eyes. The mental process behind the Cyclopean image is crucial to stereo vision. We further show with an experiment of a binocular telescope cameras and 3D display system that the image degradation introduced with turbulence can be effectively suppressed in real time sensed with human vision.

Binocular vision is a widely studied visual process in which the left and right eyes receive similar but different images with disparity. The psycho-physical visual process involves complicated and intelligent parallel imaging processing capability, including binocular summation, interaction, fusion and stereopsis.[13] If the left and right images show similar characteristics, the images may be fused in the brain to produce a Cyclopean image, i.e., a singleness of the vision. The image fusion is shown to have unique features to overcome partial image distortion, even to the extend to recover a particular image behind an obstacle.[14] Because two eyes are located in different positions on the head, an object away from fixation may have a different visual direction in each eye. When the two monocular images of the object are fused, creating a Cyclopean image, the object has a new visual direction based on the two monocular visual directions. This so-called Allelotropia is particularly interesting for overcoming image perturbation. Because visual intelligence is shown to present unique characteristics of tolerance to image dis-

*Corresponding author. Email: stszjy@mail.sysu.edu.cn

tortion, it is expected that the binocular vision should be applicable to correct image distortion appearing in long distance telescope imaging.

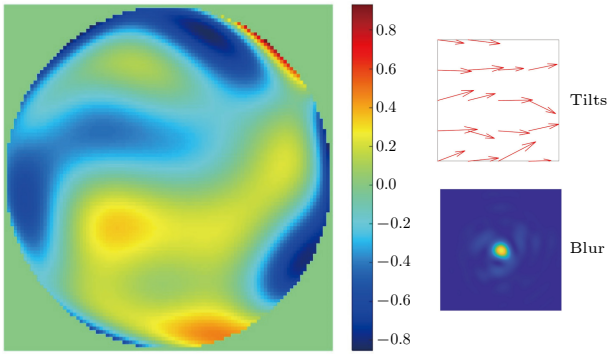

Fig. 1. Atmospheric turbulence phase screen simulated using the Zernike polynomial method.

Zernike polynomial method (the first 36 orders: further increasing the order of the Zernike polynomial can not better improve the results of image restoration) is applied in this work to generate a simulated atmospheric turbulence phase screen. The phase φ can be represent as $\varphi(\frac{D\boldsymbol{r}}{2}) = \sum_{i=1}^{N} a_i Z_i(\boldsymbol{r})$, where $\{a_i\}_{i=1}^{36}$ is the Zernike coefficients and $\{Z_i(\boldsymbol{r})\}_{i=1}^{36}$ is the Zernike basis;[15,16] D is the aperture diameter of the optical system; $\boldsymbol{r}$ is the polar coordinate vector of the unit circle. The second term a_2 and third term a_3 (x-tilt and y-tilt) of the Zernike polynomials play a role in causing image distortion in the simulation of atmospheric turbulence. The vector tilt matrix, denoted as T, can be obtained by performing a 2D Fourier transform on the wave-front tilts and multiplying by Gaussian white noise. The other higher-order terms a_4, a_5, ..., a_{36} play the role in causing image blurring in the simulation. A typical point spread function (PSF) shown on the bottom right corner of Fig. 1 is presented for the optical imaging system with the turbulence taken into account.

The degradation of an image due to atmospheric turbulence is expressed as[16]

$$\tilde{I} = \{T \circ B(\mathrm{PSF})\}(I) + n, \tag{1}$$

where $\tilde{I}$ is the degraded image affected by turbulence, I is the clean image, or original object. B is a convolution matrix that makes the image blur and T describes random shifts in image pixels that makes the image distortion. Here $\circ$ is the operation meaning the functional composition, and n is additive noise. A typical numerical simulation phase screen for an atmosphere turbulence is obtained and is presented in Fig. 1 with tilt map and tilt-free blur PSF presented in the same figure.

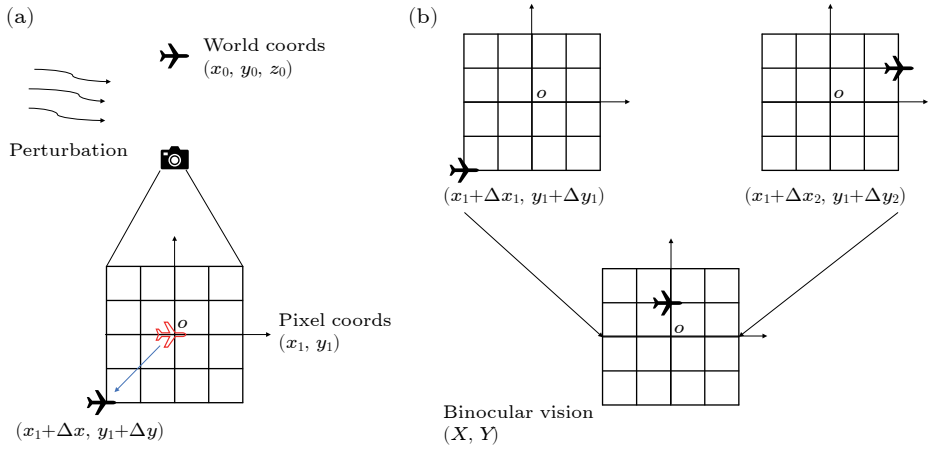

Fig. 2. Perturbed pixels perceived at a new location through binocular vision: (a) the external perturbation causing the pixel to shift within the pixel coordinate system, (b) binocular vision: horizontal and vertical binocular responses.

As shown in Fig. 2(a), a small aircraft as an image source in space with world coordinates (x_0, y_0, z_0) is considered. Using the camera's intrinsic and extrinsic parameters, its coordinates (x_1, y_1) in the pixel coordinate system can be determined.[17] External perturbation will cause the pixel to shift within the pixel coordinates. Let the deviation of perturbed pixel point away from the original unperturbed position expressed by Δx and Δy be

$$(x,\ y) = (x_1 + \Delta x,\ \ y_1 + \Delta y). \tag{2}$$

The binocular response can be characterized in terms of horizontal and vertical parts. It is noteworthy that horizontal fusion and vertical fusion occur simultaneously to avoid the appearance of diplopia, or double vision, which is the precondition for image fusion. However, horizontal and vertical fusions behave very differently, both in spatial and temporal characteristics.[18,19] When dealing with horizontal disparities, i.e., the x-axis, Cyclopean image's new direction is usually in the average direction of the two images.[12] For fusion in vertical direction, i.e., the y-axis, it is expected that the perception of vertical pixel converges to the equilibrium position due to a much slower response time with vertical fusion than with horizontal fusion.[18] Furthermore, the mechanism of vertical stabilization is also in operative for human vision with upright posture.[20,21] For the unknown vertical equilibrium posi-

tion exerted by the turbulence, it is reasonable to adopt the smaller deviation as it is closer to the equilibrium position with zero deviation. The fusion rules for binocular vision can then be summarized by the following equation:

$$\begin{aligned} X &= \text{Average}(x_\text{l},\, x_\text{r}) = \text{Average}(x_1 + \Delta x_\text{l},\;\; x_1 + \Delta x_\text{r}) \\ Y &= \text{Min}(y_\text{l},\, y_\text{r}) = \text{Min}(y_1 + \Delta y_\text{l},\;\; y_1 + \Delta y_\text{r}), \end{aligned} \tag{3}$$

where x_l, y_l, x_r, and y_r represent the pixel coordinates of the left- and right-eye images, respectively. The perception of the perturbed imaging from the left- and the right-eye images can be sensed at a new location with vision. Here, Average describes the average value, and Min describes the smaller value between y_l and y_r. Numerical simulation is carried out for an experiment consisting of a telescope, an image sensor and an autostereoscopic display with a 24-inch 1920×1080 resolution screen perceived at a viewing distance of 900 mm. The simulation parameters for the experiment are as follows: the path length L is 7 km, the aperture diameter D is 0.2034 m, the focal length d is 1.2 m, the wavelength λ is adopted as 525 nm, binocular baseline is 6.5 cm, and the image size is 512×512 pixels. With the standard visual acuity[22] defined as 20/20, we can derive that a resolution of a single pixel on the screen can be visualized.

The advantages of binocular fusion to reduce the horizontal and vertical deviation from original positions are presented in Fig. 2. With the single channel recording and display, the degree of image distortion is shown in Fig. 2(a), while the new position for distorted image is shown in Fig. 2(b) if we assume the left and right images have different distortions presented in the upper right of Fig. 2(b).

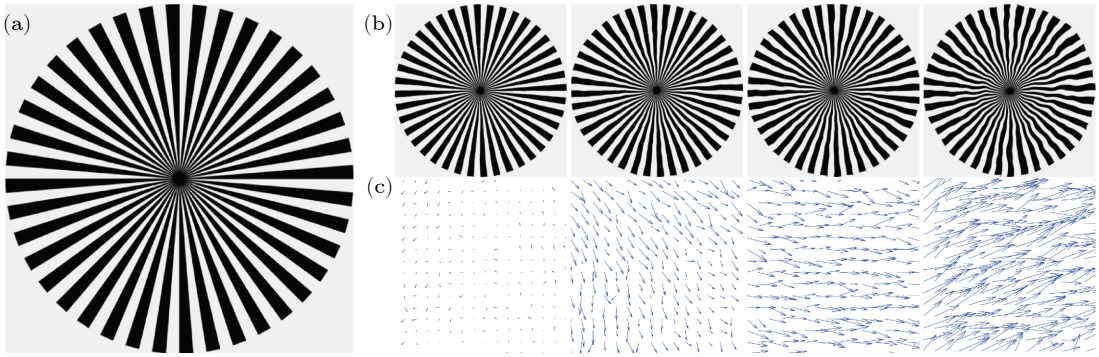

Fig. 3. Simulated images and tilt maps for $D/r_0 = 1.0699$, $D/r_0 = 2.8094$, $D/r_0 = 4.2552$, $D/r_0 = 5.4385$: (a) the clean image, (b) the simulated distorted images affected by turbulence with different D/r_0, (c) the corresponding tilt maps.

Table 1. Magnitude of pixel displacement in the X and Y directions under different D/r_0.

D/r_0	1.0699	2.8094	4.2552	5.4385
X direction	±2 pixels	±4 pixels	±7 pixels	±12 pixels
Y direction	±2 pixels	±4 pixels	±7 pixels	±12 pixels

With D and r_0[23] adopted in this simulation, the random shifts in image pixels by the atmospheric turbulence with different D/r_0 are presented for a standard image test chart as a new chart with different amounts of pixel displacement by the turbulence. The short-exposure atmospheric turbulence is simulated by sampling correlated Zernike coefficients.[15] Figures 3(a), 3(b) and 3(c) show the clean image, the simulated distorted images affected by turbulence with different D/r_0 (gradually increases from left to right), and the corresponding tilt maps, respectively. The direction of the arrows represents the direction of pixel displacement, and the size of the arrows indicates the magnitude of the pixel displacement. Table 1 presents the magnitude of pixel displacement in the X and Y directions under different D/r_0. To avoid visual fatigue and achieve visual comfort, it is recommended that the horizontal disparity fusion range should be less than 1°,[24] and the vertical fusion disparity range should be less than 0.57°.[25] According to the specifications of the 3D display unit, we can estimate that the allowable pixel ranges for horizontal and vertical fusion are 41 pixels and 24 pixels, respectively. With this numerical simulation, the pixel deviation is within the range of binocular fusion.

A pair of short-exposure turbulence-distorted images (without blur: as typical cases, we show that turbulence images under the maximal D/r_0) are adopted here for the simulation with Allelotropia so as to synthesize the Cyclopean image. Figures 4(a) and 4(b) show the left- and right-eye distorted images affected by turbulence, respectively. The Cyclopean image synthesized with Allelotropia is shown in Fig. 4(c). In comparison, Fig. 4(d) shows the image by simply adding the left- and right-eye images together, which is a standard practice to obtain an averaged image. In this case, the summation produces a 'double image' instead of a single improved image.

In order to compare the results with different post-imaging scenarios, the structure similarity (SSIM) analysis is adopted. The clean image is known and is served as a standard image. The input to SSIM consists of two images, from which we can determine the similarity between them.

The general expression of SSIM can be written as[17,26]

$$\begin{aligned}&\mathrm{SSIM}(\mathrm{img}_1,\ \mathrm{img}_2)\\&=\frac{(2\mu_{\mathrm{img1}}\mu_{\mathrm{img2}}+C_1)(2\sigma_{\mathrm{img1,\,img2}}+C_2)}{(\mu_{\mathrm{img1}}^2+\mu_{\mathrm{img2}}^2+C_1)(\sigma_{\mathrm{img1}}^2+\sigma_{\mathrm{img2}}^2+C_2)},\end{aligned}\tag{4}$$

where μ and σ represent the mean intensity and the mean variance of the images, C_1 and C_2 are two small constants. We selected 100 pairs of left and right images and calculated the average SSIM values for left-eye images, right-eye images, Cyclopean images, and summation images for four different D/r_0 values.

Compared to the left- and right-eye images, the statistical SSIM of the Cyclopean images has improved by 8.6% to 13.6%, statistically demonstrating the effectiveness of the Allelotropia effect in reducing turbulence distortion. Figure 6(a) allows for a more intuitive observation of the improvement in Cyclopean image quality through the use of the statistical SSIM curves.

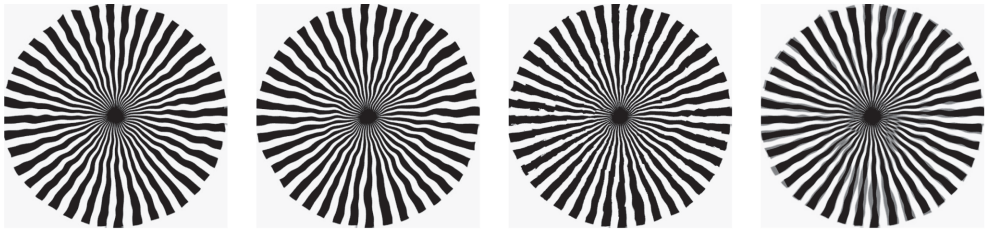

(a) Left-eye image (b) Right-eye image (c) Cyclopean image (d) Summation image

Fig. 4. Comparative results for distorted image: (a) the left-eye turbulence distorted image, (b) the right-eye turbulence distorted image, (c) the cyclopean image synthesized with Allelotropia, and (d) the summation image.

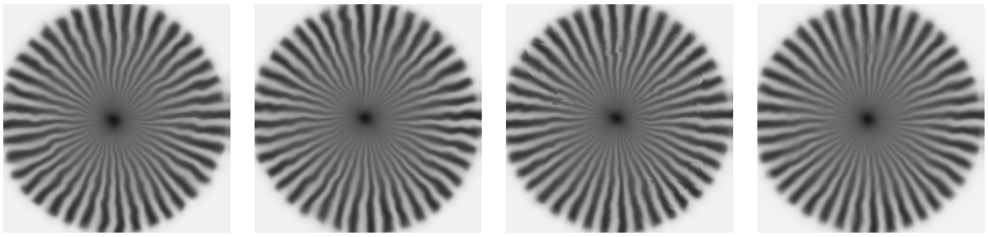

(a) Left-eye image (b) Right-eye image (c) Cyclopean image (d) Summation image

Fig. 5. Comparative results for blurred image: (a) the left-eye turbulence distorted image, (b) the right-eye turbulence distorted image, (c) the cyclopean image synthesized with Allelotropia, and (d) the summation image.

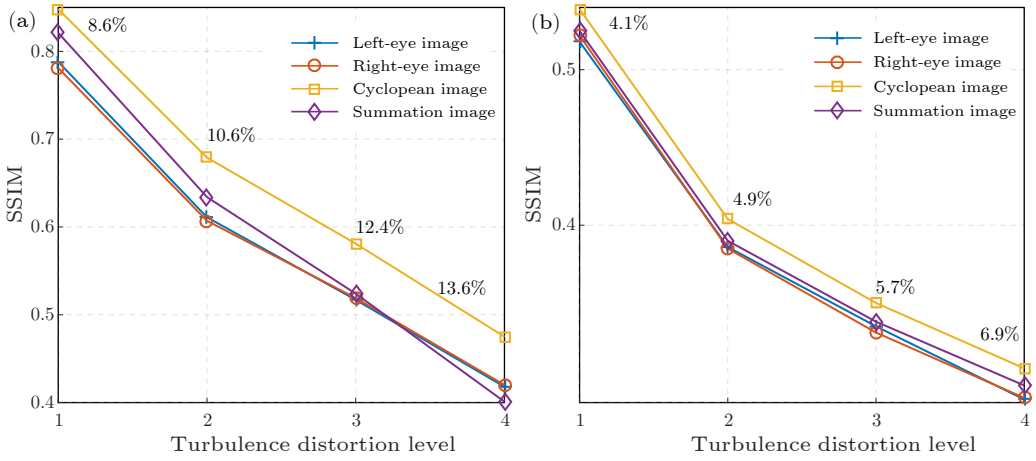

Fig. 6. Image quality analysis using SSIM curves for four different D/r_0 values about left- and right-eye images, cyclopean images, and summation images: (a) tilt without blur, (b) tilt and blur.

In order to describe the real image processing with Allellopia, we also simulated the real image by taking into account of the image blurring. In this case, we can also observe the improvement in Cyclopean image quality through the SSIM value. Figures 5(a) and 5(b) show the short-exposure images, respectively, affected by turbulence (with blur and tilt: we show turbulence images under the maximal D/r_0). Figures 5(c) and 5(d) show the cyclopean images and the summation images. The statistical SSIM curves are shown in Fig. 6(b).

To demonstrate the effectiveness of binocular vision for restoring image distortion, an experiment with a binocular telescope, sensors and an autostereoscopy is constructed. Here, the home made telescope has an aperture of 16 mm

with a focal length of 95 mm and the lens spacing is 22 mm. The sensors (Sony IMX334 CMOS) have a resolution of 3840×2160 with the size of 2 μm for a pixel, and the autostereoscopy is MID-FD24VT.[27,28] With this system, a field experiment is carried out to observe the objects 0.1–8 km away.

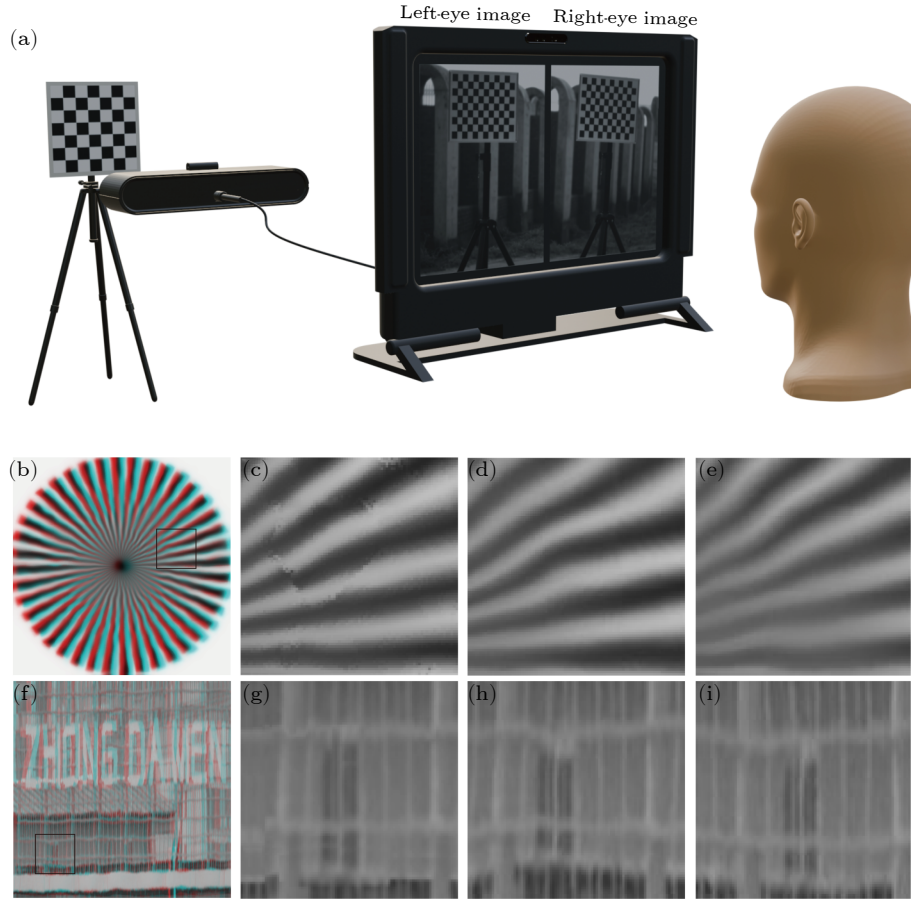

Fig. 7. Experimental proof of the effectiveness of binocular vision for restoring image distortion: (a) experimental dual channel recording, image displaying and perception with human vision; [(b), (f)] red-blue anaglyphs, i.e., (b) simulated results for a reference charter and (f) field experimental results for an object 0.5 km away; (c) the zooming restored result corresponding to (b); [(d), (e)] the corresponding left-eye image (d) and the right-eye image (e); (g) the zooming restored result corresponding to (f); [(h), (i)] the corresponding left-eye image (h) and the right-eye image (i).

The field experimental arrangement is shown in Fig. 7(a). The effect of binocular vision for distorted image recovery is most obvious with video mode when the real-time imaging presents prominent turbulence effect. One can instantly sense with the Allelotropia that the turbulence effect is substantially reduced with three-dimensional (3D) recording, displaying and perception (when the left- and right image dual input is displayed on the autostereoscopy sensed with binocular vision) compared with planar mode (either left or right channel input is disabled). The binocular perception allows a much more stable and distortion corrected image observation than with planar case, demonstrating its effectiveness in real-time reconstruction of optical imaging by suppressing the effect of atmospheric turbulence, which is in agreement with the simulation results shown in Figs. 5 and 6.

It is interesting to note that the distortion correction is operative for binocular vision both for movie and for stationary images. The dynamic response of the brain to turbulence distortion is particularly useful for many application purposes.

For the convenience of demonstrating the proof of the principle, experimental results with binocular viewing are presented with anaglyph for those without a 3D display system. By wearing red-blue glasses, one can easily observe the improvement for the simulation result shown in Fig. 7(b) and for the field experimental result shown in Fig. 7(f). The comparison can be made by covering left or right eye image and by comparing it with anaglyph perception. We also show the zooming restored results in Fig. 7(c) and Fig. 7(g) corresponding to Figs. 7(b) and 7(f), respectively [Figs. 7(d), 7(e), 7(h), and 7(i) are the corresponding left and right-eye images]. We can clearly see the improvement effect.

One interesting advantage is the observation of the system's enhanced capability to anti-vibration or anti-shaking. For 2D image 0.5 km away with conventional planar recording and display, the image perception is very

sensitive to environmental vibration. While with 3D mode, the vibration and shaking effect is substantially reduced due to the binocular Cyclopean effect.

In summary, we have demonstrated that the Allelotropia effect can effectively help suppress image distortions caused by turbulence, presenting a more robust and accurate image restoration than with planar image recording and post-processing. This study, based on the simulation and field experiment, is facilitating our conclusion by comparing SSIM values obtained with a planar recording and processing with the Cyclopean image by left- or right-eye images as input. Field experiment with real time dual channel recording and display instantly demonstrates the capability of binocular telescope observation. Hence this work could serve as guideline to develop new scenario and technique for real-time image distortion correction, which should have immediate applications in atmospheric or underwater optical imaging.

Acknowledgments. This work was supported by the National Natural Science Foundation of China (Grant No. 61991452), Guangdong Key Project (Grant No. 2020B0301030009), and the National Key Research and Development Program of China (Grant No. 2021YFB2802204).

References

[1] Qian X M, Zhu W Y, Wang A T, Gu C, and Rao R Z 2010 *Chin. Phys. Lett.* **27** 044214
[2] Keller J B 1962 *Wave Propagation in Random Media. Proc. Sympos. Appl. Math.* (Providence, R.I.: American Mathematical Society) vol XIII pp 227–246
[3] Fleagle R G and Businger J A 1981 *An Introduction to Atmospheric Physics* (San Diego: Academic)
[4] Beckers J M 1993 *Annu. Rev. Astron. Astrophys.* **31** 13
[5] Wang F J, He H X, Zhuang H C, Xie X S, Yang Z C, Cai Z G, Gu H Y, and Zhou J Y 2015 *Biomed. Opt. Express* **6** 2237
[6] Anantrasirichai N, Achim A, Kingsbury N G, and Bull D R 2013 *IEEE Trans. Image Process.* **22** 2398
[7] Fried D L 1978 *J. Opt. Soc. Am.* **68** 1651
[8] Zhuang H C, He H X, Xie X S, and Zhou J Y 2016 *Sci. Rep.* **6** 32696
[9] Chen B, Geng Z X, Shen J, and Yang Y 2009 *Chin. Phys. Lett.* **26** 040701
[10] Tong X, Xu R J, Xu P F, Zeng Z S, Liu S X, and Zhao D M 2023 *Adv. Photon.* **5** 066003
[11] Cheng J M, Zhu W Y, Li J Y, Xu G, Chen X W, and Yao C 2023 *Photonics* **10** 666
[12] Hariharan-Vilupuru S and Bedell H E 2009 *Vis. Res.* **49** 190
[13] Skalicky S E 2016 *Binocular Single Vision and Stereopsis.* In: *Ocular and Visual Physiology* (Singapore: Springer) p 355
[14] Karim S, Tong G, Li J Y, Qadir A, Farooq U, and Yu Y T 2023 *Inform. Fusion* **90** 185
[15] Chimitt N and Chan S H 2020 *Opt. Eng.* **59** 083101
[16] Noll R J 1976 *J. Opt. Soc. Am.* **66** 207
[17] Huang Y R, Liu Y K, Liu H S, Shui Y Y, Zhao G W, Chu J H, Situ G H, Li Z B, Zhou J Y, and Liang H W 2021 *Photonics* **8** 454
[18] Perlmutter A L and Kertesz A E 1978 *Vis. Res.* **18** 219
[19] Kerstez A E and Perlmutter A L 1983 *IEEE Trans. Biomed. Eng.* **BME-3** 246
[20] Nardon M, Pascucci F, Cesari P, Bertucco M, and Latash M L 2022 *Neuroscience* **500** 79
[21] Kapoula Z and Lê T T 2006 *Exp. Brain Res.* **173** 438
[22] Cline D, Hofstetter H W, and Griffin J 1997 *Dictionary of Visual Science* 4th edn (Boston: Butterworth-Heinemann)
[23] Roggemann M C and Welsh B M 2018 *Imaging through Turbulence* (New York: CRC Press)
[24] Chiba S 2006 *ITE Tech. Rep.* **30** 21 (in Japanese)
[25] Kooi F L and Toet A 2004 *Displays* **25** 99
[26] Wang Z, Bovik A C, Sheikh H R, and Simoncelli E P 2004 *IEEE Trans. Image Process.* **13** 600
[27] He Y, Chen X H, Zhang G Y, Fan Y J, Liu X B, Deng D Y, Yan Z B, Liang H W, and Zhou J Y 2024 *Displays* **82** 102651
[28] Zhang A Q, Chen X H, Wang J H, He Y, and Zhou J Y 2024 *Micromachines* **15** 403